Research Square

Preprints are preliminary reports that have not undergone peer review.
They should not be considered conclusive, used to inform clinical practice,
or referenced by the media as validated information.

Solvent-Regulated Hydrogen-Bond Competition in Hyperelastic, Adhesive Organogels

Jiazheng Bao
The University of Texas at Austin
Jin Yang
The University of Texas at Austin
Donglei Emma Fan
dfan@austin.utexas.edu

The University of Texas at Austin

Research Article

Keywords:

Posted Date: July 10th, 2026

DOI: https://doi.org/10.21203/rs.3.rs-10295760/v1

License: This work is licensed under a Creative Commons Attribution 4.0 International License.
Read Full License

Additional Declarations: The authors declare no competing interests.

Solvent-Regulated Hydrogen-Bond Competition in Hyperelastic, Adhesive Organogels

Jiazheng Bao[a], Jin Yang[a, b], Donglei Emma Fan[a, c, *]

a. Materials Science and Engineering Program, Texas Materials Institute, The University of Texas at Austin, Austin, Texas, USA, 78712
b. Department of Aerospace Engineering and Engineering Mechanics, The University of Texas at Austin, Austin, TX, USA 78712
c. Department of Mechanical Engineering, The University of Texas at Austin, Austin, Texas, USA, 78712

Correspondence and requests for materials should be addressed to the authors: Donglei Emma Fan (dfan@austin.utexas.edu).

Abstract

Hydrogen-bonded polymer gels are attractive because reversible bonding associations dissipate energy, support recovery, and promote adhesion. In the current swollen gels, however, solvent environments often fail to dynamically modulate these interactions, frequently resulting in unbalanced competition among polymer-polymer, polymer-solvent, and solvent-solvent interactions. Consequently, although hydrogen-bonded networks offer a pathway to reversible energy dissipation, their mechanical performance is frequently limited by kinetically trapped, rigid polymer states. Herein, we report a general material design strategy for the synthesis of hyperelastic, high-strength adhesive gels governed by active regulation of solvent-mediated hydrogen-bond competition. By exploring polar aprotic solvents that can effectively regulate the balance between inter-chain polymer–polymer associations and polymer–solvent interactions, we achieve a controlled transition from dense, collapsed network architectures to highly solvated, dynamic systems. Using poly(acrylic acid) (PAA) as a model polymer, we show that dimethylformamide (DMF) acts as an active hydrogen-bond acceptor, facilitating exceptional tensile deformability exceeding 6,000% and exceptional interfacial adhesion. The reported solvent-regulation strategy can be expanded to diverse polar aprotic solvents, yielding a series of gels that retain high stretchability, while offering strong adhesion. Organogels designed and optimized through the reported approach could serve as a new class of gel platform, relevant to soft robotic components, stretchable adhesive joints, damping layers, gel electrolytes, and particle-binding matrices for battery electrodes.

Introductions

Hydrogen bonding has been widely used to introduce reversible, dynamic molecular interactions in soft polymer networks, enabling energy dissipation, recovery, adhesion, and environmental responsiveness.[1–5] However, hydrogen-bonded polymer networks are highly sensitive to their solvent environment.[6–8] In swollen gels, solvent molecules can compete with polymer-polymer hydrogen bonds and change both the strength and lifetime of reversible polymer-polymer chain association.[9,10] While strong polymer-polymer self-association can reinforce the overall network, excessive physical crosslinking may restrict chain mobility and kinetically trap the polymer chains, thereby limiting large-scale deformation.[11–14] Thus, the mechanical response of a hydrogen-bonded gel depends not only on the polymer structure, but also on how the surrounding solvent modulates the hydrogen-bonding equilibrium.

To actively modulate this equilibrium, solvent selection becomes critical. Polar aprotic solvents are polar liquids that accept hydrogen bonds but do not donate them.[15] These solvents play broad roles in polymer materials, from polymer processing and organogel formation to ion gels and gel electrolytes.[16,17] While properties such as solvent polarity, hydrogen-bond accepting ability, and low volatility are known to influence swelling, solvent retention, segmental mobility, and ion transport, direct participation of these solvents in modulating polymer hydrogen bonding has received much less attention compared to their conventional roles, such as macroscopic swelling media or plasticizers. Within polymer systems, polar aprotic solvent molecules can both swell the network and interact directly with hydrogen-bonding polymer groups as exclusive hydrogen-bond acceptors. This distinction is important because this specific donor-acceptor interaction can change the balance between polymer-solvent and polymer-polymer hydrogen bonds, potentially permitting the network to dissipate energy, rearrange under deformation, and recover after unloading.[13,18–24] Therefore, we hypothesize that solvent-dependent hydrogen-bond competition enables a route to a new class of organogels whose deformation, recovery, and adhesion emerge from dynamic interplay between polymer association and solvent participation.

We herein validate this hypothesis, reporting a general strategy for the synthesis of hyperelastic and strongly adhesive organogels (Fig. 1A), governed by solvent-mediated hydrogen-bond regulation. Unlike traditional approaches that primarily utilize solvents as structural diluents, this design utilizes polar aprotic solvents to actively modulate the competitive balance between inter-chain polymer–polymer associations and polymer–solvent interactions. We explore this concept in poly(acrylic acid) (PAA)-dimethylformamide (DMF) organogels, where the solvent functions as a dynamic hydrogen-bond acceptor. Our findings suggest that such a solvent-driven competitive microenvironment indeed facilitates a transition from a dense, collapsed polymer state to a highly solvated, dynamic network, thereby enabling exceptional tensile deformability exceeding 6,000% alongside superior adhesive ability. Extending this approach to Dimethyl

sulfoxide (DMSO), N-Methylpyrrolidone (NMP), dimethyl isosorbide (DMI) and γ-Valerolactone (GVL) solvents further establishes that polar aprotic solvation provides a generalizable platform for creating PAA organogels with tunable mechanical and adhesive properties. Collectively, the efforts identify polar aprotic solvation as an active contributor to the macroscopic mechanical response of organogels, offering a new gel platform for resilient soft robotic components, stretchable adhesive joints, and high-performance energy-storage interfaces.

Results

Design and Fabrication: Solvent-Regulated Organogels

The gel is designed by one-step polymerization of a solution containing monomer (acrylic acid, AA), crosslinker (N,N'-methylenebis(acrylamide), MBAA), photoinitiator (Irgacure 2959, I2959), and dimethylformamide (DMF). By introducing polymer–solvent interactions that compete with inter- and intra-chain polymer–polymer associations, the solvent actively modulates the local hydrogen-bonding environment (**Fig. 1a**). This process yields a uniform, transparent PAA-DMF organogel within 30 s (**Fig. 1d, Video S1**), which suggests a homogeneous network formation without macroscopic phase separation. Within this system, the carboxylic acid groups on the PAA chains act as hydrogen-bond donors, whereas the DMF solvent molecules provide hydrogen-bond acceptors. As a result, the PAA chains exhibit a dynamic equilibrium between self-association via polymer–polymer hydrogen bonding and association with DMF via polymer–solvent donor–acceptor interactions. These competing interactions form the molecular basis of the solvent-regulated dynamic physical network.

Thermodynamic energy calculation of these competing interactions with density functional theory (DFT) calculations supports the foundational feasibility. Further spectroscopic characterizations experimentally validate their presence. Specifically, DFT results reveal that the binding energies of the hydrogen-bonded complexes (**Fig. 1c**), follow the sequence of AA–AA single hydrogen bond, AA–DMF complex, and AA–AA cyclic dimer. The results indicate that the polymer–solvent interaction is energetically comparable to the self-association of the polymer chains, thereby enabling the solvent to effectively participate in dynamic hydrogen bond formation, modulating the physical polymer network.

Furthermore, Fourier-transform infrared (FTIR) spectroscopy of the AA–DMF mixture reveals distinct shifts in the vibrational bands associated with the carbonyl and hydroxyl groups relative to pristine AA, indicating an altered hydrogen-bonding environment (**Fig. 1e, Fig. S1**). This is further supported by ^{13}C NMR spectra (**Fig. 1f, g**), where the chemical shift of the carboxyl carbon changes upon the introduction of DMF. Collectively, these results support our hypothesis that DMF is not an inert diluent, but rather an active participant that regulates the local electronic

environment and polymer–polymer associations, thereby providing fundamental evidence for the proposed molecular design approach for creating the solvent-regulated gel.

Mechanical robustness and structural evolution

The mechanical performances of the PAA-DMF organogels are initially regulated by tuning the covalent crosslinker concentration (**Fig. 2a-c, Fig. S2a-d**). Representative tensile stress—strain curves reveal that the MBAA percentage significantly influences the balance among stretchability, stiffness, and strength (**Fig. 2b**). At a crosslinker content of only 0.05 mol%, the gel sustains exceptional tensile deformation, achieving strains exceeding 6,000%. Incremental additions of MBAA progressively increase both the modulus and peak stress, reaching a tensile strength of approximately 352 kPa, although lowering the extensibility to ~1,000%. Measurements of material shear modulus, peak stress, and strain at peak stress further support this crosslinker-dependent trade-off between elastic reinforcement and large-strain deformability (**Fig. 2c, Note S1**). Furthermore, the remarkably large-deformation capacity of the gel is demonstrated through macroscopic stretching and inflation demonstrations (**Fig. 2d,e, Video S2-3**). The material can be subjected to extensive uniaxial elongation without catastrophic rupture (**Fig. 2d**). When seamlessly attached to an inflatable balloon, the gel maintains its conformability during ~20-fold surface expansion, highlighting its capacity to accommodate substantial biaxial deformation alongside complex substrate areal and curvature changes (**Fig. 2e**). These performances not only demonstrate the gel's robust, exceptional deformability across diverse modes, but also suggest the presence of pronounced, enabling energy-dissipation mechanisms.

To elucidate the role of the physical network played in the mechanical performance, we systematically study the polymer and solvent compositions in controlled mechanical outcomes (**Fig. 2f,g**). For example, elevating the PAA concentration from 50 to 70 wt.% yields a substantial increase in both peak stress and modulus, alongside a reduction in strain (**Fig. 2f, Fig. S3**). More importantly, modulating the solvent composition reveals an important role of DMF (**Fig. 2g, Fig. S4a-c**). Although water is a well-established “good” solvent for PAA [25], the purely aqueous gel is stiff and non-ideal for elongation. Interestingly, as the DMF content progressively increases toward a pure organogel, the elongation drastically increases, while the inverse is observed for mechanical strength. This distinction suggests that increasing DMF changes the solvation environment of PAA chains, e.g., reducing the compact chain association, thereby increasing chain mobility and large-strain deformability.

We further perform cyclic tensile loading-unloading tests (**Fig. 2h**). The gel withstands consecutive deformation cycles up to 1,500% strain without observable rupture. The result suggests that the internal physical polymer network association can dynamically reconfigure to accommodate the cyclic strain over a long duration.

The structural evolution of the PAA-DMF network during deformation is further investigated via molecular dynamics (MD) simulations (**Fig. 2i-k, Fig. S5**). As shown in **Figure 2i**, the simulated polymer network elongates progressively along the tensile axis, accommodating the deformation up to a stretching ratio of λ = 3.0. Quantitative analysis shows that, despite this significant macroscopic elongation, the total number of hydrogen bonds per frame, including both PAA-DMF and PAA-PAA interactions, remains remarkably stable (**Fig. 2j, Fig. S6**). Spatial mapping of the hydrogen-bond density indicates that associative, hydrogen-bond-rich regions persist robustly throughout the stretching process (**Fig. 2k**). The obtained results can likely be attributed to the dynamic behavior of the hydrogen bonds, where dissociation-reformation events predominate during stretching, allowing the network to rearrange without losing overall structural integrity. The work points towards a dynamic solvent-mediated hydrogen-bond network that reorganizes during deformation.

Solvent-regulated hydrogen-bond redistribution and network relaxation

To elucidate the molecular interactions underlying the PAA-DMF gel's unique behaviors, non-covalent interaction (NCI) analysis is used to compare three representative interaction states: PAA-DMF association, interlocked PAA-PAA carboxylic-acid pairing, and PAA-PAA association (**Fig. 3a**). Reduced density gradient plots display attractive regions in all three states, indicating that COOH-DMF solvation and PAA-PAA carboxylic-acid association can coexist within the protonated PAA network (**Fig. 3b**). It supports a distributed hydrogen-bonding microenvironment in which both polymer-solvent and polymer-polymer associations are thermodynamically feasible in forming the network.

To confirm the presence of solvent-regulated competition, we carry out temperature-variable transmission IR spectroscopy measurements from 20 to 60 °C. The one-dimensional spectra of the O-H stretching $\nu(\mathrm{O\text{-}H})$ region capture a macroscopic heat-induced shift in this competitive balance, evidenced by the decreased intensity and blue-shift of hydrogen-bonded species alongside an increase in free COOH (**Fig. 3c**). To resolve the specific sequence of these dynamic rearrangements, two-dimensional correlation spectroscopy (2DCOS) is subsequently employed (**Fig. 3d,e, Fig. S7**).[2,9,26,27] Synchronous (Φ) and asynchronous (Ψ) spectra are generated to monitor the synchronized and unsynchronized variations in spectral intensities at specific wavenumbers. Notably, the asynchronous spectrum effectively deconvolutes the broad infrared continuum into distinct sub-populations, and the application of Noda's rules establishes a sequential thermal response order of $3{,}250\ \mathrm{cm^{-1}}(\mathrm{strongly\ bonded}) \rightarrow 3{,}400\ \mathrm{cm^{-1}}(\mathrm{medium\ bonded}) \rightarrow 3{,}550\ \mathrm{cm^{-1}}(\mathrm{free\ COOH})$ (where the arrow denotes a prior or earlier response; details are provided in **Table S1-2**). This sequence indicates that the most strongly bonded COOH groups reorganize first, progressing through intermediate states before ultimately changed into free COOH, providing strong evidence that the heat-induced rearrangement of the

PAA-DMF network is governed by a solvent-regulated competition between polymer-polymer and polymer-solvent hydrogen bonding.

Time-temperature superposition (TTS) is then used to examine the temperature-dependent relaxation of the PAA-DMF gel (**Fig. 3f,g, Fig,S8, Fig. S10, Note S2**). The shifted frequency-sweep data form continuous $G'$and G'' master curves spanning approximately six orders of magnitude for the tested frequencies, reflecting a highly versatile dynamic response that persists over a broad range of spectral timescales (**Fig. 3f, Note S2**). The temperature dependence of the empirically derived horizontal shift factors is well described by an Arrhenius relationship, with an apparent activation energy of 61.3 kJ mol^{-1} (**Fig. 3g-i, Fig. S11, Fig. S12**). This value is comparable to the energy scale expected for cooperative hydrogen-bond rearrangement,[2] suggesting that thermally activated bond reconfiguration makes a major contribution to the observed macroscopic relaxation of the PAA-DMF network. To complement these frequency-domain observations, the shear relaxation modulus $G(t)$, measured following the application of a step strain, further elucidates the stress relaxation behavior of the PAA organogel (**Fig S9**). The $G(t)$ curve continuously decreases spanning over five decades in time, eventually approaching a non-zero equilibrium modulus G_{eq}, which suggests the presence of a permanent covalent network (**Note S3**). Notably, G_{eq} accounts for only approximately 1% of the initial modulus, suggesting that the mechanical response is predominantly governed by reversible interactions rather than the covalent network. Overall, these combined rheological behaviors point toward a broad spectrum of dynamic relaxation modes, which likely stem from the diverse energy landscape of the hydrogen-bonding interactions and the inherent structural heterogeneity within the organogel network.

To further elucidate the aforementioned molecular competitive interactions, chain-level analysis is performed utilizing MD simulations of dilute solutions, comparing pure DMF, pure water, and a 1:1 DMF/water mixture. (**Fig. 3j,k**, **Note S4**). Typical conformation morphology and radius-of-gyration distributions are obtained, which demonstrate that a water-rich environment tends to drive PAA toward a collapsed, compact chain state -- driven largely by water-mediated hydrogen-bond networks pushing the polymer chains out, while a DMF-rich environment promotes a solvated and extended chain conformation (**Fig. 3j,k**). This is confirmed by the Small-angle X-ray scattering (SAXS) and Wide-angle X-ray scattering (WAXS) scattering profiles, which show the reduction of dense interchain correlation with the increase of DMF (**Fig. 3l, Fig. S13, Fig. S14**). Given that dense interchain association imposes rigid, entanglement-like physical states, the observations also suggest that DMF thermodynamically reduces water-induced chain densification, thereby supporting a dynamic, solvated PAA network. To further evaluate the effect of the DMF/H_2O solvent composition on the dynamics of this PAA network, stress relaxation tests were conducted to compare the time evolution of the normalized modulus, $G(t)/G_0$, across different solvent ratios (**Fig 3m**, **Note S3, Fig S15**). All samples exhibit a rapid initial relaxation

followed by a slowly decaying plateau, indicating the presence of multi-scale network rearrangements within the system. Notably, as the DMF ratio increases from 0:5 to 5:0, the relaxation curves shift downward globally, accompanied by a significant decrease in modulus retention after 1800 s. This behavior suggests a reduction of the residual elastic network in DMF-rich systems, where stress appears to be more readily dissipated through polymer segmental motions, reversible hydrogen bond reorganizations, and rearrangements of the local solvation environment.

Altogether, the study of the temperature-variable 1D/2D IR spectroscopy and stress relaxation measurements provides strong evidence that the temperature-controlled hydrogen-bond redistribution in DMF gels, supporting the proposed hypothesis of dynamic-bonding-enabled elastic gels.

Solvent-regulated interfacial adhesion

For a hydrogen-bonded gel, its adhesive capability to a substrate depends on both interfacial polymer-chain rearrangement and its intrinsic chemical affinity (**Fig. 4a**).[28] In-*situ* lap-shear measurements show that the interfacial adhesion is highly solvent-dependent, agreeing with this understanding (**Fig. 4b**). Compared with the water-based PAA gels, the PAA-DMF gels exhibit a much larger shear displacement and substantially enhanced peak shear stress of ~1 MPa. This drastic contrast observed in experimental characterization indicates that PAA gel adhesion is not governed solely by the interfacial COOH group. Rather, the solvent environment also plays a crucial role in regulating chain mobility, determining whether PAA chains can reorganize sufficiently to establish a mechanically robust interfacial contact. The strong adhesion of DMF-solvated PAA gels can therefore be attributed to the enhanced flexibility of the polymer chains, which facilitates optimal interfacial adaptiveness (**Fig. 4a**).

The dependence of adhesion on covalent crosslinking density further highlights the critical role of a balanced network architecture (**Fig. 4c,d**). In the absence of the MBAA crosslinker, the gel exhibits weak adhesive performance, suggesting that an insufficiently connected polymer network lacks the bulk cohesion required to sustain large-scale interfacial deformation. At 0.05 mol% MBAA, both adhesion strength and interfacial fracture energy increase steeply. However, further increasing the MBAA concentration reduces the interfacial adhesion. This trend suggests that while a baseline network is necessary for stress transfer, excessive permanent crosslinking restricts adaptive chain rearrangement, thereby diminishing interfacial engagement.

Thus, the robust interfacial adhesion of PAA gel on a surface can be achieved through optimized DMF-PAA solvation, combined with tailored network crosslinking, wherein the PAA chains offer both sufficient interfacial adaptiveness and reversible bonding with various surfaces. As a demonstration of this adaptability, the PAA-DMF gel adheres conformably to a human finger,

even under dynamic joint movement (**Fig. S16**). Furthermore, the gel exhibits strong and reversible adhesion across a diverse range of hydrophobic and hydrophilic substrates, including glass, wood, poly(ethylene terephthalate) (PET), nylon, polyester, poly(methyl methacrylate) (PMMA), carbon fiber, and polyvinyl chloride (PVC) (**Fig. S17, Video S4**). The synergistic balance between interfacial mobility and bulk network integrity facilitates durable adhesion under repeated mechanical deformation, as observed (**Fig. 4e-h**). Consequently, the PAA-DMF gel sustains a 3.2 kg hanging load and maintains stable cyclic shear responses over 1000 cycles at shear strains of ±10%, ±15%, and ±20%. The nearly overlapping stress profiles after hundreds of cycles indicate the strong mechanical integrity and exceptional fatigue resistance of the adhesive interface.

Generalizable strategy for creating an array of high-extension, adhesive gels

The solvent-regulation mechanism observed in the PAA-DMF system can be effectively applied to a broader series of polar aprotic solvents. We further demonstrate the generalizability of the working mechanism by preparing PAA organogels with GVL, DMI, DMSO, and NMP—four polar aprotic solvents with distinct molecular structures and hydrogen-bond-accepting environments (**Fig. 5a**). The resulting organogels exhibit pronounced solvent-dependent mechanical behaviors (**Fig. 5b,c, Fig. S19**). PAA-GVL exhibits the highest Ogden modulus and peak stress among the various systems, while PAA-NMP reaches the maximum elongation prior to failure. PAA-DMI yields a more compliant stress-strain dependence, and PAA-DMSO shows reduced ductility. These varying mechanical responses indicate that the stiffness, strength, and extensibility of aprotic solvent-based PAA organogels can be systematically tuned by modulating the solvent type and its composition, a phenomenon that is likely attributable to the varied solvent-polymer interaction strengths.

Consistent with the robust interfacial adhesion achieved in the DMF-solvent-enabled PAA system, the extended solvent series also generates strong interfacial adhesion properties (**Fig. 5d,e**). PAA-DMI demonstrates the highest peak adhesion strength, while PAA-NMP offers the largest work of adhesion. To evaluate the durability of the adhesive interface, cyclic shear measurements are performed on porcine skin (**Fig. 5f**), which demonstrate highly stable, nearly-unchanged shear stress over 1000 loading cycles. The animal-skin demonstration shows the potential of the reported solvent-regulated adhesive gels for practical applications.

Finally, we perform theoretical calculation and spectroscopy characterization, as detailed in **Fig. 5g-k**, **Fig. S20** and **Note S5**. Rather than merely confirming phenomenological observations, these computational and experimental findings systematically elucidate the underlying molecular interactions, thereby supporting the feasibility of the solvent-regulation principle across a broader set of polar aprotic PAA organogels.

Discussion

We propose a general principle for designing and fabricating a new class of hyperelastic and adhesive gels based on aprotic solvents. We validate the principle by synthesizing organogels with hyperelasticity and strong adhesion through an easy, one-step method. The formation of such gels suggests that the mechanical performance of a polymer network relies on the active competition between polymer-polymer and polymer-solvent interactions. Whereas a conventional hydrogen-bonded gel is mainly governed by polymer-polymer associations, a PAA-DMF organogel is regulated by competing polymer-polymer and polymer-solvent hydrogen-bonding interactions. Here, DMF acts not as a passive swelling medium but as an active hydrogen-bond acceptor that modulates the local bonding environment of PAA chains. We further extend the concept and create a series of hyperelastic, adhesive gels using different polar aprotic solvents, including DMI, DMSO, GVL and NMP. They are highly stretchable, transparent, and super adhesive. The work opens a pathway for a new gel platform that could find applications ranging from fatigue-resistant, optically clear adhesives, controlled drug-release soft surfaces, robotics, and stretchable ionotronics.

Figure 1

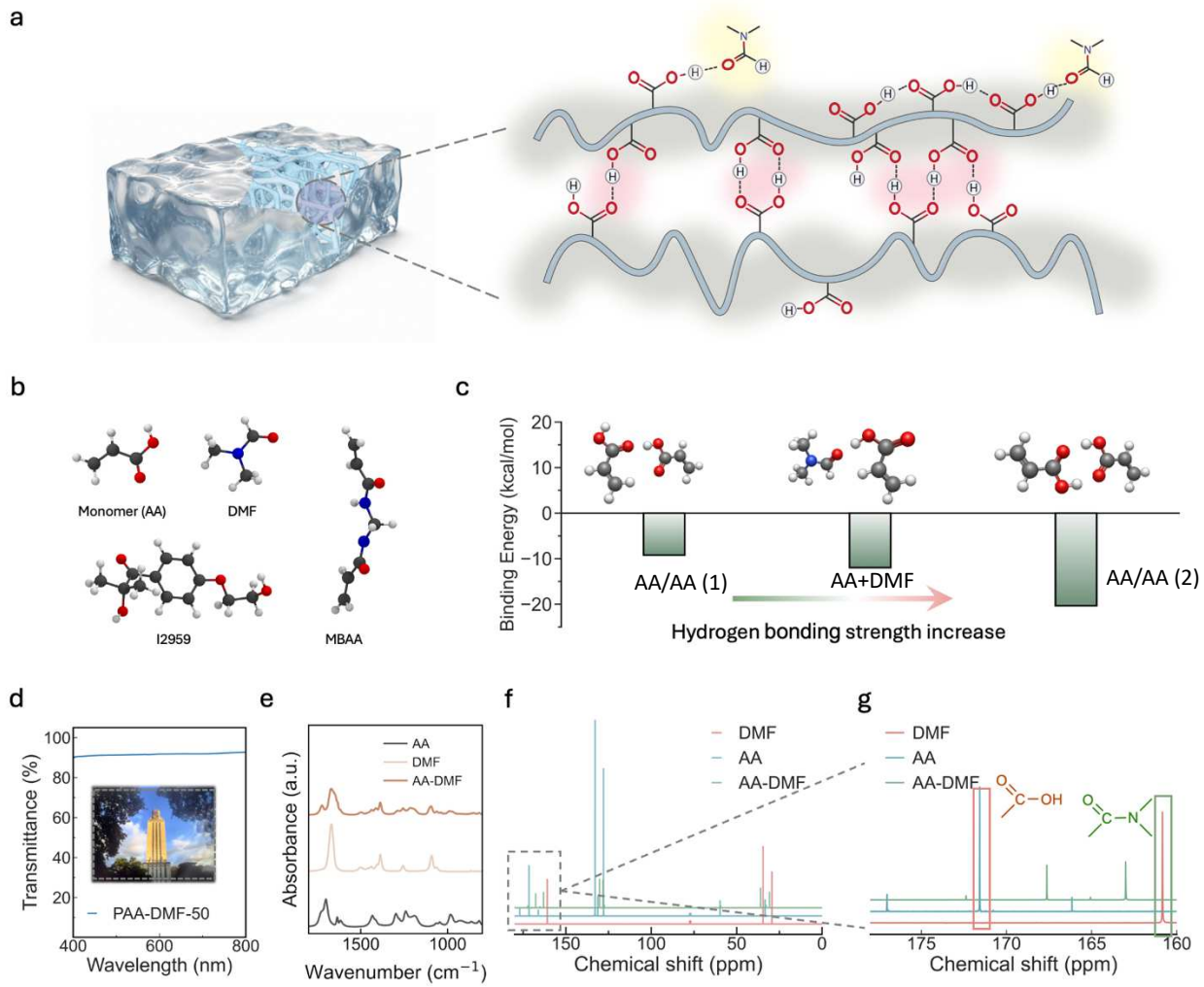


Figure 1 | Molecular design principle: solvent-regulated PAA-DMF organogels.

a, Schematic of the design principle for solvent-regulated H-bond competing interaction. In hydrogen-bonded polymer gels, dominant polymer-polymer associations can lead to local network locking, whereas an active solvent introduces polymer-solvent interactions that compete with polymer-polymer associations, regulating the dynamic physical network. **b**, Molecular structures of the monomer (PAA), solvent (DMF), crosslinker (MBAA), and photoinitiator (12959) for *in-situ* photopolymerization of PAA-DMF organogels. **c**, DFT-calculated binding energies of representative hydrogen-bonding complexes, showing that DMF-carboxylic acid interactions provide a comparable energetic basis for polymer-solvent competition. **d**, Optical transparency of PAA-DMF organogel. **e**, FTIR spectra of AA, DMF, and AA-DMF mixtures, revealing changes in hydrogen-bonding environments. **f, g**, ^{13}C NMR spectra and enlarged carboxyl-carbon region of DMF, AA, and AA-DMF, showing changes in the local electronic environment of carboxyl groups

upon interaction with DMF. Together, these results support DMF as an active solvent regulator that mediates competing polymer-polymer and polymer-solvent hydrogen-bonding interactions in PAA-DMF organogels.

Figure 2

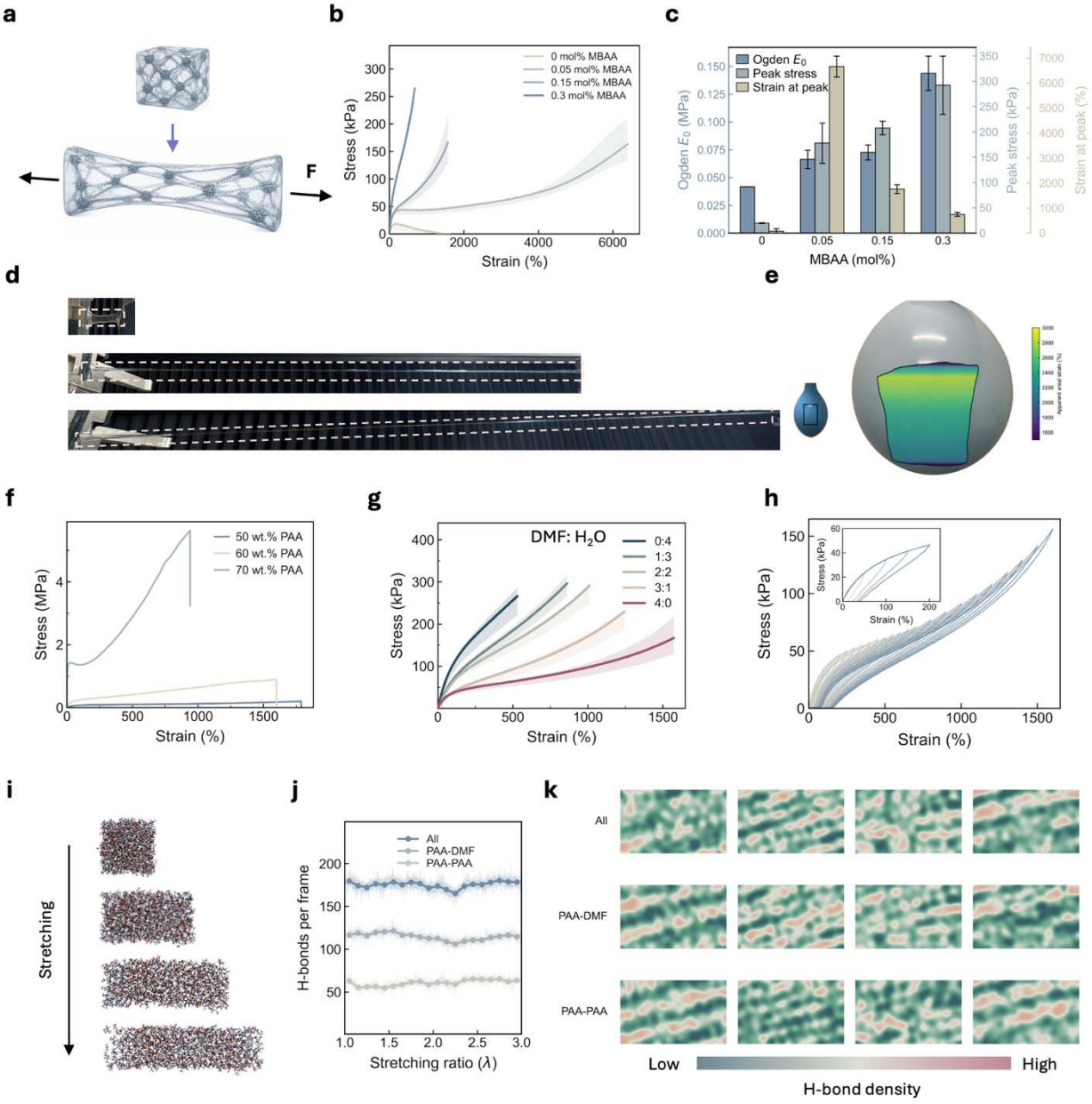


Figure 2 | Tunable mechanical properties and large-deformation tolerance of PAA-DMF organogels.

a, Schematic of the deformation of a sparsely covalently crosslinked PAA-DMF organogel. **b,** Representative tensile stress-strain curves of organogels prepared at different MBAA contents. **c,** Ogden modulus, peak stress, and strain-at-peak at different MBAA contents: the effect of covalent crosslink density on mechanical performance. **d,** large uniaxial stretching and **e,** conformal deformation on an inflatable balloon with stable adhesion. Apparent strain distribution mapped

in color. **f,** Tensile stress-strain curves at different PAA concentrations and **g,** DMF:H_2O ratios. The latter indicates that water content tunes the solvent-mediated network, which reshapes the mechanical response. **h,** Cyclic loading-unloading showing hysteresis and recoverable deformation. **i,** Molecular dynamics snapshots of PAA-DMF network under a stretching process. **j,** Number of hydrogen bonds during continuous stretching, separated into total, PAA-DMF, and PAA-PAA contributions. **k,** Normalized H-bond center density maps visualize the spatial texture of the H-bond network during stretching, extracted from MD simulations at 1.0, 1.5, 2.0, and 2.5 in stretch ratio (λ) (left to right). Rows (top to bottom) show all H-bonds followed by the contributions from PAA-DMF and PAA-PAA.

Figure 3

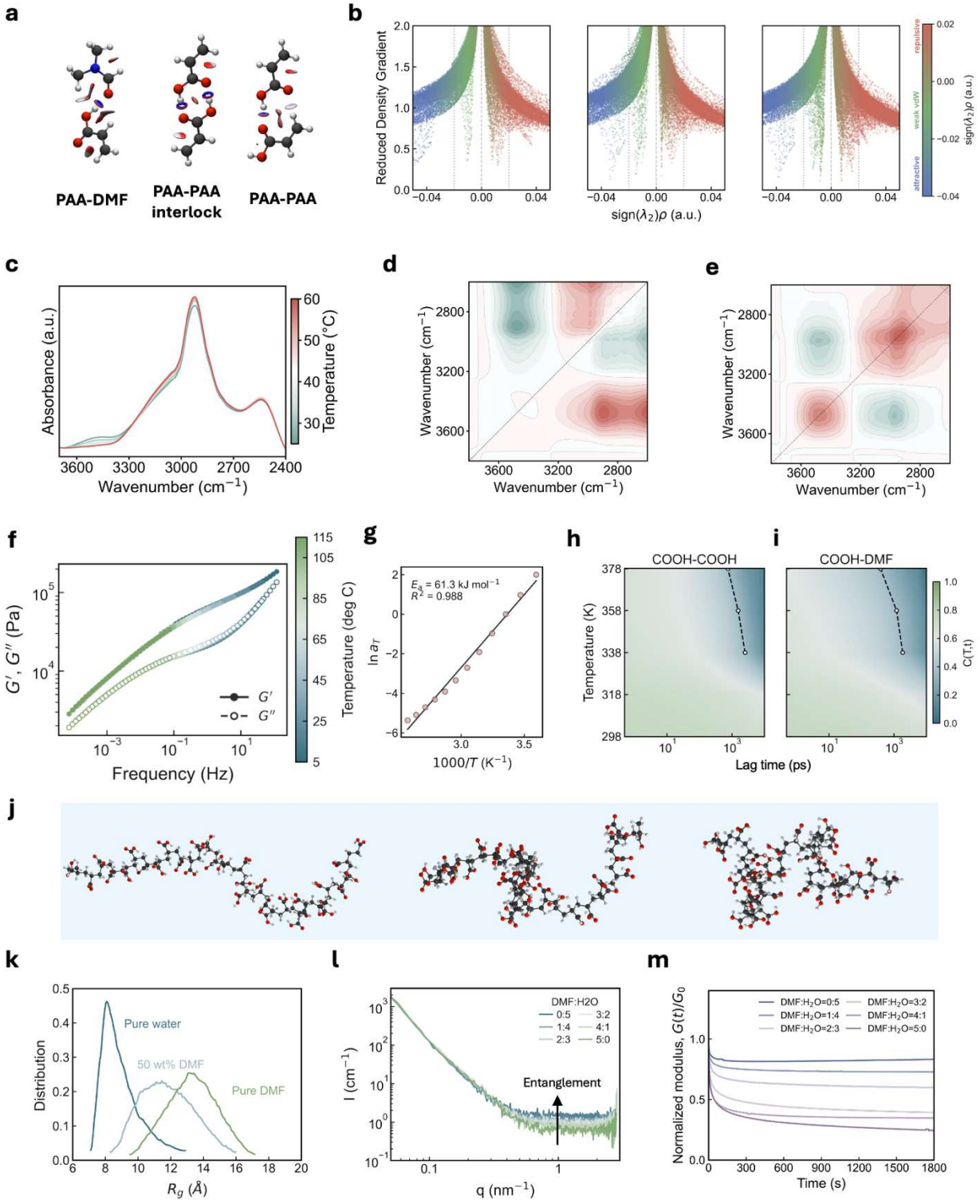


Figure 3 | DMF-mediated solvation converts dense PAA association into a dynamic, exchangeable network.

a,b, Reversible PAA-DMF and residual PAA-PAA interactions as competing local states in the PAA network based on DFT-optimized interaction motifs and reduced-density-gradient analyses. **c-e,** Variable-temperature FTIR and 2D correlation spectroscopy reveal thermally responsive redistribution of O-H/C-H-associated hydrogen-bond environments, indicating dynamic exchange rather than fixed bonding states. **f,g,** Temperature-dependent rheology shows broad, thermally activated relaxation of the PAA-DMF network. **h,i,** Molecular dynamics correlation analyses compare COOH-COOH and COOH-DMF interaction lifetimes, supporting a dynamically exchangeable DMF-solvated carboxyl environment. **j,k,** Chain conformations and radius-of-gyration distributions show that DMF maintains a more solvated and extended PAA chain state, whereas water-rich controls drive compact chain association. **l,** Scattering profiles further show that increasing DMF suppresses the dense interchain correlation associated with water-induced chain packing. **m,** Stress-relaxation fitting confirms a broad relaxation spectrum with a finite long-time elastic contribution. Both experiments and calculations support that DMF acts as an active solvation regulator: it competes with compact PAA-PAA association, preserves dynamic COOH-DMF exchange, and enables network relaxation in the PAA-DMF organogel.

Figure 4

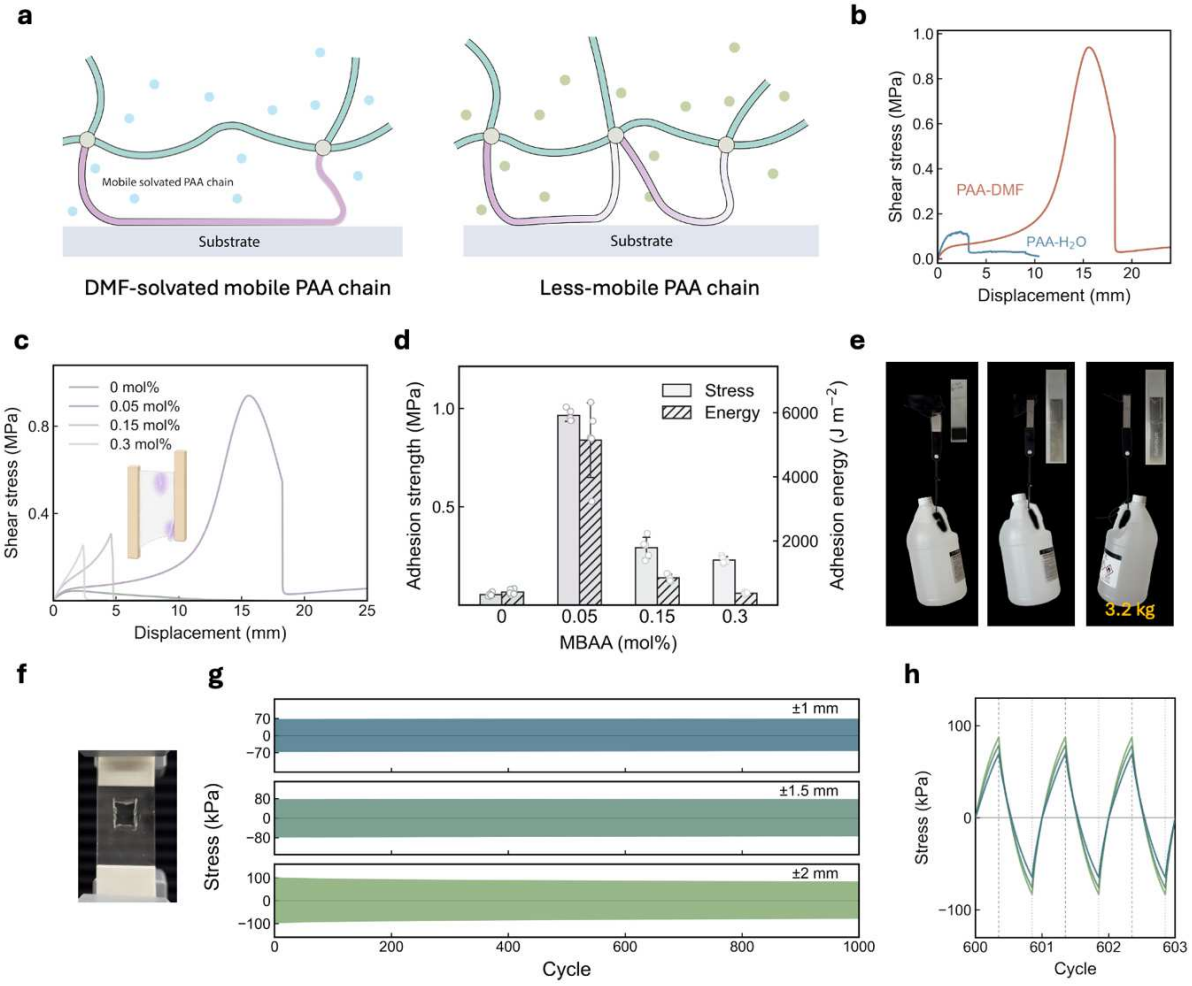


Figure 4 | Surface-adaptive adhesion performance.

a, Schematic comparison of highly mobile DMF-solvated PAA chains and less-mobile PAA chains at a solid substrate interface. DMF solvation enables chain rearrangement and conformal surface contact, whereas reduced chain mobility limits interfacial adaptation. **b,** Representative lap-shear stress-displacement curves comparing PAA-DMF and PAA-H_2O gels on glass. **c,** Representative lap-shear curves of PAA-DMF gels with different MBAA contents. **d,** Adhesion strength and energy versus MBAA concentration, showing the optimized adhesion performance at 0.05 mol% MBAA. **e,** Load-bearing demonstration of the PAA-DMF gel adhered to aluminum and steel substrates (15 mm x 25 mm), suspending a 3.2 kg weight. **f,** Photograph of the bonded gel specimen used for cyclic adhesion testing. **g,** Adhesion stability over 1000 cycles under cyclic shear displacement amplitudes of ±1, ±1.5, and ±2 mm using a 10 × 10 mm bonded area at 100 mm min^{-1}. **h,** Representative stress-cycle profiles from cycles 600-603, showing stable cyclic stress response.

Figure 5

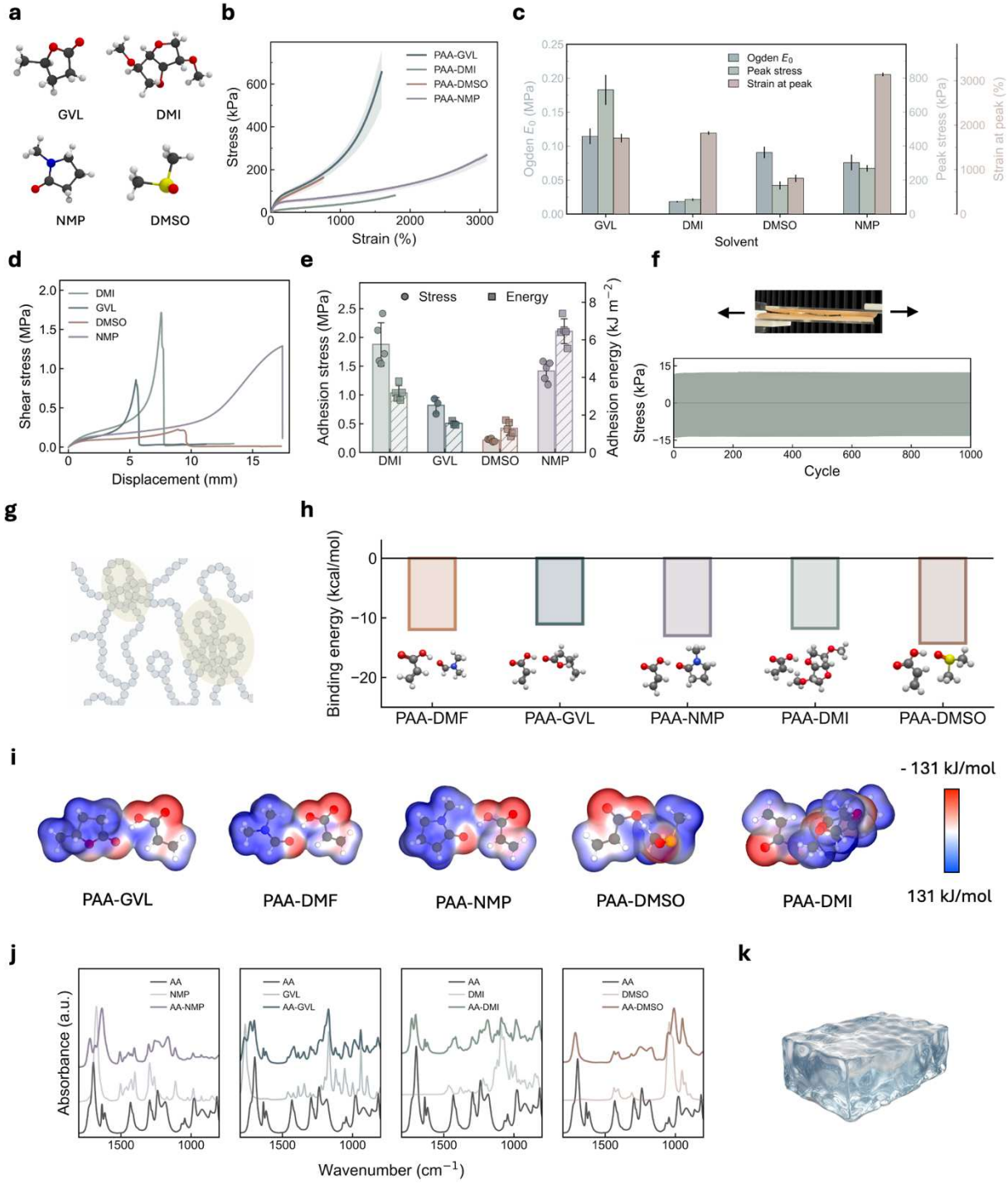


Figure 5 | Solvent-regulation principle validated in an array of polar aprotic solvents. PAA organogels prepared using an array of polar aprotic solvents show tunable mechanical and adhesive behavior. **a,** Molecular structures of the employed polar aprotic solvents. **b,** Representative tensile stress-strain curves of PAA organogels with different solvents. **c,**

Comparison of Ogden modulus, peak stress, and strain at peak. **d,** Representative lap-shear curves. **e,** Quantified adhesion stress and adhesion energy. **f,** Cyclic loading response showing stable stress over 1000 cycles. **g,** Schematic illustration of solvent-regulated competing interactions within PAA networks. **h,** DFT-calculated binding energies between acrylic acid and solvent molecules. **i,** Electrostatic potential maps of representative acrylic acid-solvent complexes. **j,** FTIR spectra of acrylic acid, solvents, and acrylic acid-solvent mixtures, showing solvent-dependent spectral features.

Methods

Synthesis of various gels

The glassy gels were fabricated by a one-step polymerization. In a typical procedure, a specified concentration of AA (for example, C_m = 50 wt.%), covalent crosslinker of MBAA (0.1 mol%, in a concentration relative to C_m) and photoinitiator of I2959 (0.05 mol%, in a concentration relative to C_m) were dissolved in DMF to form a uniform solution. The solution was then poured into a mould sandwiched between two pieces of glass separated by a spacer and then cured under ultraviolet light (60 $m\,Wcm^{-2}$) for 10 min to obtain the DMF gel. The other organogels and hydrogels were fabricated in the same process by replacing the solvents or monomers.

Tensile test

Unless otherwise stated, uniaxial tensile tests were performed using an Instron 68FM-100 Universal Testing Machine equipped with a 100 N load cell at RT of 23 ± 2°C and RH of 30 ± 10%. Both ends of the samples were glued with an additional layer of DMF gels with a thickness of 1~2 mm to reduce the slippage, and then clamped by the clamps with an initial length of 10 ± 1 mm. Unless otherwise stated, all of the tensile tests were performed at a loading rate of 100 mm min^{-1}. Cyclic tensile stress-strain curves were performed at loading and unloading rates of 500 mm min^{-1} with a relaxation time of 1 min under no force between two cycles. Young's modulus was calculated from the initial slope of the stress-strain curves. Samples for compression stress-strain tests were cylinders with a diameter of 10 mm and a height of 10 mm. Unless otherwise stated, cyclic compression stress-strain curves were performed at loading and unloading rates of 100 mm min^{-1} with a relaxation time of 1 s between two cycles. Each mechanical test was repeated with at least three individual samples.

Lap-shear adhesion test

The lap-shear measurements of organogels were performed using an Instron 68FM-100 at a speed of 5 mm min^{-1}. For the adhesion test, two pieces of glass slides (Corning) were rinsed with deionized water. The gel with a size of 10 mm × 10 mm and a thickness of 0.6 mm was prepared by injecting the precursor solution into the reaction cell consisting of the two pretreated glass slides and a PDMS spacer, followed by UV polymerization for 5 min. Each mechanical test was repeated with at least five individual samples.

Dynamic mechanical analysis

The storage and loss moduli were measured by an oscillatory shear plate rheometer (TA ARG2). The thickness of the organogel was 1 mm, and the gel was cut into a cylinder with a diameter of

12 mm. The applied axial force was 1 N, and the frequency sweeping was carried out in the 0.1-100 rad s^{-1} ω range at a constant shear strain of 5%.

NMR Characterization

^{13}C NMR spectra of various monomers, ionic liquids and their mixtures in $CDCl_3$ were recorded using a Bruker spectrometer MR400.

Transmittance test

Rectangle samples (width = 20 mm, length = 20 mm, and thickness = 2 mm) were used to measure the transmittance of various gels using a UV–Vis–NIR spectrometer (PE Lambda 950, Perkin Elmer) with a wavelength range of 400–800 nm.

FTIR tests

The chemical structures of various materials were analyzed using FTIR spectroscopy (Bruker Invenio FTIR). All spectra were measured in transmission mode, with data recorded in the range of 4,000-800 cm^{-1} over 32 scans.

Two-dimensional correlation spectroscopy (2DCOS)

The temperature-variable transmission IR spectra of the organogel from 20 to 60 °C were used for performing 2D correlation analysis. The software 2D Shige ver. 1.3 (©Shigeaki Morita, Kwansei Gakuin University, Japan, 2004–2005) was used for 2D correlation analysis, and Python script was further used to draw contour maps. In 2DCOS spectra, red colors represent positive intensities, while blue colors represent negative intensities.

In-situ small-angle X-ray scattering and wide-angle X-ray scattering during stretching gels

In-situ SAXS/WAXS measurements during tensile deformation were performed to monitor the structural evolution of the PAA-DMF organogel under stretching. Gel strips were mounted on a tensile stage and stretched uniaxially to a maximum strain of 1000%. SAXS and WAXS patterns were collected at selected strain levels during deformation. The two-dimensional scattering patterns were corrected for background scattering and converted to one-dimensional profiles for further analysis.

In-situ small-angle X-ray scattering at different temperatures

Temperature-dependent small-angle X-ray scattering (SAXS) measurements were performed to monitor the thermal structural evolution of the PAA-DMF organogel. Gel samples were sealed in a temperature-controlled sample holder to minimize solvent evaporation during heating. SAXS profiles were collected at selected temperatures from room temperature to 100 °C after thermal

equilibration at each temperature. The scattering intensity was recorded as a function of the scattering vector q, and the background signal was subtracted before analysis.

Time-temperature superposition rheology

Temperature-dependent oscillatory shear measurements were performed using a rheometer equipped with an 8 mm parallel-plate geometry. To minimize sample-to-sample variation, a single PAA-DMF organogel specimen was utilized throughout the entire temperature sequence. Angular frequency sweeps were conducted from 0.1 to 100 rad s^{-1} at each temperature, applying a fixed strain amplitude of 5% to ensure the testing remained within the linear viscoelastic (LVE) regime.

Measurements were recorded across a temperature range of 5 to 65 °C, designating 25 °C as the reference temperature. Prior to each frequency sweep, the sample was allowed to equilibrate at the target temperature until both the system temperature and normal force completely stabilized. To mitigate solvent evaporation at elevated temperatures, a solvent trap equipped with a DMF reservoir was employed. Furthermore, measurements were strategically repeated at selected temperatures to verify thermal reversibility and confirm sample integrity throughout the heating protocol.

Time-temperature superposition (TTS) was executed by horizontally shifting the isothermal storage modulus G' and loss modulus G''curves along the angular frequency axis to construct master curves referenced to 25 °C. The horizontal shift factors (a_T) were determined by optimizing the overlap of both G' and G'' across the accessible frequency range. The apparent activation energy associated with the temperature-dependent relaxation process was subsequently derived by fitting these shift factors to the Arrhenius relationship:

$$\ln a_T = \frac{E_a}{R}\left(\frac{1}{T} - \frac{1}{T_{\text{ref}}}\right)$$

where E_a is the apparent activation energy, R is the universal gas constant, T is the absolute measurement temperature, and T_{ref} is the absolute reference temperature.

References

1. Zhou, N., Cui, T., Lei, Z. & Wu, P. Bioinspired learning and memory in ionogels through fast response and slow relaxation dynamics of ions. *Nat Commun* **16**, 4573 (2025).
2. Ye, H., Wu, B., Sun, S. & Wu, P. Self-compliant ionic skin by leveraging hierarchical hydrogen bond association. *Nat Commun* **15**, 885 (2024).
3. Wu, B., Wei, P., Sun, S. & Wu, P. Fatigue-free artificial ionic skin toughened by self-healable elastic nanomesh. *Nat Commun* **13**, 4411 (2022).
4. Zhang, W., Wu, B., Sun, S. & Wu, P. Skin-like mechanoresponsive self-healing ionic elastomer from supramolecular zwitterionic network. *Nat Commun* **12**, 4082 (2015).
5. Shi, X. *et al.* Phase transition driven tough hydrogel ionic thermoelectric cell with giant thermopower. *Nat Commun* **16**, 9002 (2025).
6. Jin, Z., Liu, Y. & Wang, C. Molecular Design of Ion-Dipole Interactions for Flexible Ionic Conductors. *CCS Chem* **7**, 3569–3590 (2025).
7. Yaakub, S. N. *et al.* Non-invasive ultrasonic neuromodulation of the human nucleus accumbens impacts reward sensitivity. *Nat Commun* **16**, 10192 (2025).
8. Zheng, S. *et al.* Pressure-stamped stretchable electronics using a nanofibre membrane containing semi-embedded liquid metal particles. *Nat Electron* **7**, 576–585 (2024).
9. Chen, L. *et al.* A hyperelastic hydrogel with an ultralarge reversible biaxial strain. *Science* **383**, 1455–1461 (2024).
10. Zheng, Y. *et al.* How chain dynamics affects crack initiation in double-network gels. *Proc. Natl. Acad. Sci. U.S.A.* **118**, e2111880118 (2021).

11. Wang, Z. *et al.* Toughening hydrogels through force-triggered chemical reactions that lengthen polymer strands. *Science* **374**, 193–196 (2021).
12. Fukao, K. *et al.* Hydrogels toughened by biominerals providing energy-dissipative sacrificial bonds. *J. Mater. Chem. B* **8**, 5184–5188 (2021).
13. Guo, X. *et al.* A skin-mimicking multifunctional hydrogel via hierarchical, reversible noncovalent interactions. *Science Advances* (2025).
14. Wang, M. *et al.* Glassy gels toughened by solvent. *Nature* **631**, 313–318 (2024).
15. Jordan, A., Hall, C. G. J., Thorp, L. R. & Sneddon, H. F. Replacement of Less-Preferred Dipolar Aprotic and Ethereal Solvents in Synthetic Organic Chemistry with More Sustainable Alternatives. *Chem. Rev.* **122**, 6749–6794 (2022).
16. Zhang, X., Li, T., Wang, Z., Wang, J. & Zhao, S. Polar aprotic solvent-resistant nanofiltration membranes generated by flexible-chain binding interfacial polymerization onto PTFE substrate. *Journal of Membrane Science* **668**, 121294 (2023).
17. Greco, F. A. Polar, aprotic solvents and the hydrophobic effect. *J. Phys. Chem.* **88**, 3132–3133 (1984).
18. Zhang, X. *et al.* Hydro-locking in hydrogel for extreme temperature tolerance. *Science* **387**, 967–973 (2025).
19. Zhang, C., Ren, Z., Liu, L. & Yin, Z. Modelling hydrogen bonds in*NN*-dimethylformamide. *Molecular Simulation* **39**, 875–881 (2013).
20. Yuk, H. *et al.* Dry double-sided tape for adhesion of wet tissues and devices. *Nature* **575**, 169–174 (2019).

21. Pan, Z. *et al.* Designing nanohesives for rapid, universal, and robust hydrogel adhesion. *Nat Commun* **14**, 5378 (2023).
22. Hao, X. P. *et al.* Healable, Recyclable, and Multifunctional Soft Electronics Based on Biopolymer Hydrogel and Patterned Liquid Metal. *Small* **18**, 2201643 (2022).
23. Feng, X. *et al.* Polymer informatics: Current status and critical next steps. *Materials Science and Engineering: R: Reports* **144**, 100595 (2021).
24. Guo, S. *et al.* Precisely manipulating polymer chain interactions for multifunctional hydrogels. *Matter* **8**, 101785 (2025).
25. Wang, M. *et al.* Tough and stretchable ionogels by in situ phase separation. *Nat. Mater.* **21**, 359–365 (2022).
26. Li, C. *et al.* Photoswitchable and Reversible Fluorescent Eutectogels for Conformal Information Encryption. *Angew Chem Int Ed* **62**, e202313971 (2023).
27. Li, T. *et al.* Robust skin-integrated conductive biogel for high-fidelity detection under mechanical stress. *Nat Commun* **16**, 88 (2025).
28. Xue, Q., He, X., Lei, J., Hong, W. & Yang, C. Synergizing network topology and solvent compatibility for gels with hyperelasticity and omniadhesion. *Science Advances* (2026).